Rapid ion-implantation-induced amorphization of $In_xGa_{1-x}As$ relative to InAs and GaAs

Z. S. Hussain*
Department of Electronic Materials Engineering, Research School of Physics and Engineering, Australian National University, Canberra ACT 0200, Australia

E. Wendler and W. Wesch
Friedrich-Schiller-Universität Jena, Institut für Festkörperphysik, Max-Wien-Platz 1, D-07743 Jena, Germany

G. J. Foran
Australian Nuclear Science and Technology Organisation, Menai NSW 2234, Australia

C. S. Schnohr, D. J. Llewellyn, and M. C. Ridgway
Department of Electronic Materials Engineering, Research School of Physics and Engineering, Australian National University, Canberra ACT 0200, Australia

(Received 10 May 2008; revised manuscript received 10 December 2008; published 4 February 2009)

We report on the rapid implantation-induced amorphization of the ternary $In_xGa_{1-x}As$ alloys. Unlike $Al_xGa_{1-x}As$, $In_xGa_{1-x}As$ did not exhibit amorphization kinetics intermediate between the two binary-alloy extremes. Instead, our investigation of the crystalline-to-amorphous phase transformation over the entire stoichiometry (x) range demonstrated that $In_xGa_{1-x}As$ alloys with $x=\sim 0.06-0.53$ were rendered amorphous at fluences less than that required for both InAs and GaAs. Implantation-induced disorder was quantified with Rutherford backscattering spectroscopy in the channeling configuration and fit to the Hecking model to yield the probabilities of direct-impact and stimulated amorphizations. The phase transformation was dominated by stimulated amorphization, which was a maximum at the stoichiometry ($x=\sim 0.34$) most easily amorphized, while the probability of direct-impact amorphization was effectively stoichiometry independent. From extended x-ray-absorption fine-structure spectroscopy measurements of unimplanted $In_xGa_{1-x}As$ alloys, separate stoichiometry-dependent In-As and Ga-As bond lengths were measured. Distortion in both the bond-length and bond-angle distributions was apparent though structural perturbation was primarily accommodated in the latter as consistent with measured deviations from the tetrahedral bond angle. We attribute the relative ease with which the $In_xGa_{1-x}As$ alloys were amorphized to the presence of localized regions of strain due to structural distortion. Equivalently, atomistic configurations comprised of strained bond lengths and bond angles represent pre-existing and preferential sites for stimulated amorphization. To demonstrate the general applicability of our model, we report on preliminary measurements with the $In_xGa_{1-x}P$ alloys which also exhibit a bimodal bond-length distribution and distortion in the bond-angle distribution. Comparable amorphization behavior to that of the $In_xGa_{1-x}As$ alloys has been observed.

DOI: 10.1103/PhysRevB.79.085202 PACS number(s): 61.43.Dq, 61.72.uj, 61.72.Cc, 61.05.cj

I. INTRODUCTION

The use of $In_xGa_{1-x}As$ in electronic and photonic device fabrication[1–6] has generated considerable interest in this ternary alloy where material properties can be precisely tailored by varying the stoichiometry x. The resulting properties are generally intermediate between the two binary extremes[7,8] including, for example, a band gap that progressively decreases as x increases. In contrast, we have previously reported that both $In_{0.53}Ga_{0.47}As$ (Ref. 9) and $In_{0.20}Ga_{0.80}As$ (Ref. 10) are rendered amorphous by ion implantation at fluences lower than those required for both InAs and GaAs. For this paper, we have studied the ion-implantation-induced amorphization of $In_xGa_{1-x}As$ over the entire stoichiometry range with the aim of identifying the factors responsible for these intriguing amorphization kinetics.

Though amorphous-layer formation in $In_xGa_{1-x}As$ by ion implantation has been previously investigated by several authors,[11–13] the rapid amorphization behavior was not apparent in the absence of a comparison with both InAs and GaAs. Akano *et al.*[11] compared disorder and dynamic annealing processes in $In_{0.53}Ga_{0.47}As$ and InP as functions of implantation temperature and flux and reported that $In_{0.53}Ga_{0.47}As$ was more difficult to amorphize than InP. Yu[12,13] studied amorphous-layer formation in $In_xGa_{1-x}As$ for $x=0-0.5$ and suggested that a homogeneous amorphization process was operative at room temperature in the presence of significant dynamic annealing. In contrast, a heterogeneous process dominated at liquid-nitrogen implant temperatures where dynamic annealing was much reduced.

We now present a more detailed investigation of amorphous-layer formation in $In_xGa_{1-x}As$ implanted at room temperature over the entire stoichiometry range (including the two binary alloys). Using Rutherford backscattering spectroscopy in the channeling configuration (RBS-C), we deduce the stoichiometry most easily amorphized and identify the mechanism governing the amorphization process. Using extended x-ray-absorption fine-structure (EXAFS) spectroscopy, we determine the bond-length and bond-angle distributions for $In_xGa_{1-x}As$ as well as InAs, GaAs, $Al_{0.50}Ga_{0.50}As$, and $In_xGa_{1-x}P$ and compare structural distortion in these materials. Correlating the RBS-C and EXAFS

results, we then discuss the factors responsible for the amorphization behavior of the ternary $In_xGa_{1-x}As$ alloys relative to both InAs and GaAs and then extend our model to the $In_xGa_{1-x}P$ alloys.

II. EXPERIMENTAL

Epitaxial $In_xGa_{1-x}As$ layers with $x=0.06$, 0.28, 0.37, 0.53, 0.75, and 0.90 were grown by metal-organic chemical-vapor deposition (MOCVD) on (100) substrates. Stoichiometries of $x=0.06$, 0.28, and 0.37 were grown on GaAs, $x=0.53$ and 0.75 were grown on InP, while $x=0.90$ was grown on InAs. The substrate material was chosen to minimize lattice mismatch between the substrate and epitaxial layer and hence reduce the misfit dislocation density. The thickness of the epitaxial layers was 0.10 ± 0.01 μm with the exception of lattice-matched $In_{0.53}Ga_{0.47}As$ where the layer was 0.6 μm thick. Nominally undoped InAs, GaAs, and $In_xGa_{1-x}As$ samples were then implanted simultaneously with 60 keV ^{74}Ge ions at room temperature. RBS-C was used to measure the implantation-induced disorder on the In sublattice for $In_xGa_{1-x}As$ and InAs samples and on the Ga/As sublattices for GaAs samples. RBS-C measurements were performed along the ⟨100⟩ direction with 2.0 MeV He ions and a scattering angle of 168°. A lesser scattering angle would have yielded superior depth resolution but inferior mass resolution. Our choice of scattering angle was governed by the need to avoid the overlap of scattering contributions from In and Ga/As atoms within the implanted layer.

From the RBS-C spectra, the quantity $\Delta\chi_{min}$ was calculated using $\Delta\chi_{min}=(Y_{implanted}-Y_{unimplanted})/(Y_{random}-Y_{unimplanted})$, where $Y_{implanted}$ and $Y_{unimplanted}$ are the integrated backscattered ion yields in the channeling direction for the implanted and unimplanted samples, respectively, and Y_{random} is the random yield. $\Delta\chi_{min}$ is an approximate measure of lattice disorder. A $\Delta\chi_{min}$ value of zero corresponds to unimplanted material while a value of one represents no epitaxial alignment consistent with amorphous material. The backscattered ion yield was integrated over a depth range (typically 50–350 Å) where the implantation-induced vacancy production determined from SRIM 2003 (Ref. 14) decreased to two-thirds of the maximum value. Figure 1 shows representative RBS-C spectra of $In_{0.53}Ga_{0.47}As$ (0.6 μm thick) as functions of fluence, showing only scattering contributions from the In sublattice. The conversion from backscattered ion energy to depth was performed using the DICADA program.[15] Clearly an increase in fluence resulted in an increase in backscattered ion yield consistent with the progression of the crystalline-to-amorphous phase transformation.

For ease of comparison, the ion fluence N_I was converted to the number of displacements per lattice atom, η_{dpa}, where $\eta_{dpa}=N_{displ}N_I/N_0$. N_{displ} is the number of displacements per ion per angstrom calculated with SRIM and N_0 is the atomic density of the corresponding material. In the SRIM simulations, displacement energies of 25 eV were used for all atoms. $\Delta\chi_{min}$ data as functions of η_{dpa} were fitted to the defect interaction and amorphization model of Hecking *et al.*[16,17] to determine the probabilities for direct-impact and stimulated amorphizations, P_a and A_s, respectively. In general, a decrease in P_a yields an increase in slope, while a decrease in A_s shifts the curve to higher η_{dpa} values. As $\Delta\chi_{min}$ approaches one, the slope approaches zero, yielding significant ambiguity in quantifying the η_{dpa} value required for complete amorphization. Given the subtle differences in the amorphization kinetics of the $In_xGa_{1-x}As$ alloys presented below, we have sought to reduce the uncertainty in our comparative study by defining the "critical η_{dpa}" as the inflection point of the Hecking fit.

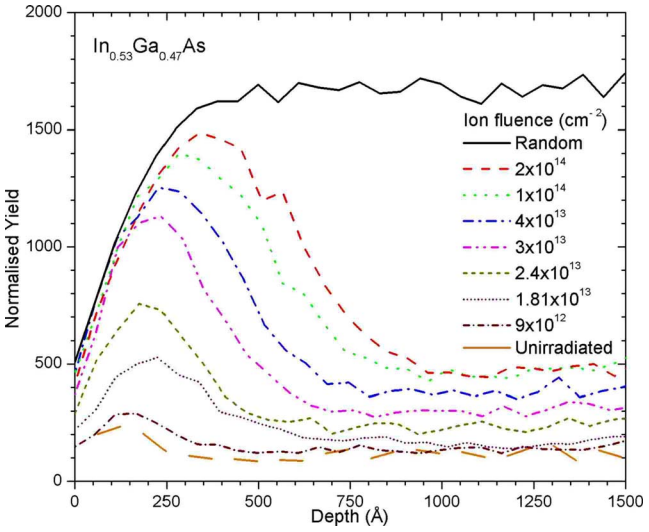

FIG. 1. (Color online) RBS-C spectra of $In_{0.53}Ga_{0.47}As$ irradiated at room temperature as functions of the number of displacements per atom.

EXAFS measurements of unimplanted material were performed in fluorescence mode at the In, Ga, and As *K* edges using beamline 20-B in the Photon Factory, Japan. (311) and (111) monochromators—the latter detuned by 50%—were utilized at the In and Ga/As edges, respectively. Prior to the EXAFS measurements, the epitaxial $In_xGa_{1-x}As$ layer was separated from the substrate by dissolving the latter using a selective chemical etchant ($HCl:H_2O$ and $H_2O_2:NH_4OH$ to dissolve InP and GaAs, respectively)[18–22] and then mounted on Kapton tape. In the absence of a grazing-incidence configuration, removal of the substrate was necessary to eliminate contributions from In, Ga, and/or As atoms in the substrate to the measured EXAFS spectra of the ternary alloy layers. Furthermore, this method yielded a significant reduction in x-ray scattering and, as a consequence, the fluorescent signal of interest comprised a much greater fraction of the total signal incident on the solid-state detector. Fluorescence spectra were collected with a 36-element Ge pixel array detector with the sample aligned at 45° to the incident x-ray beam and maintained at 10 K to minimize thermal vibrations. ATHENA was used for background removal and normalization of the fluorescence spectra. Structural parameters were then determined with ARTEMIS over a photoelectron wave-number (k) range of 3–15 $Å^{-1}$ and a non-phase-corrected radial distance (r) range of 1.7–4.5 Å. Both ATHENA and ARTEMIS are part of the IFEFFIT (Refs. 23 and 24) code for EXAFS data analysis. For each sample, the In, Ga, and As spectra were fitted simultaneously with the bond

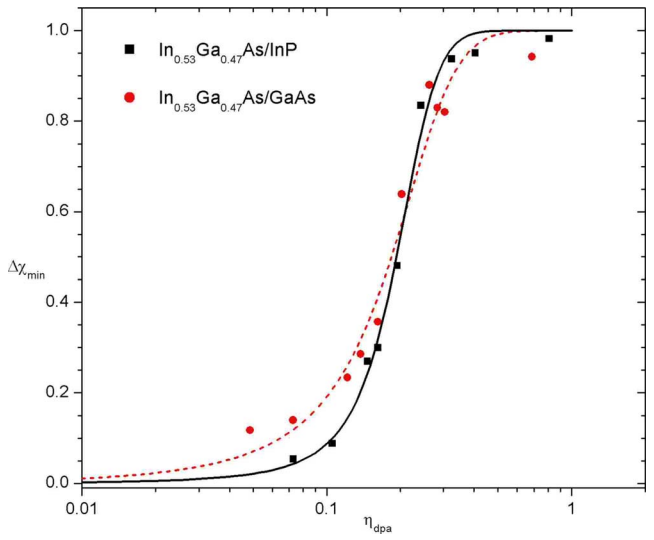

FIG. 2. (Color online) $\Delta\chi_{\min}$ as a function of the number of displacements per atom comparing $In_xGa_{1-x}As$ grown on InP and GaAs. The plotted curves are fits to the experimental data points.

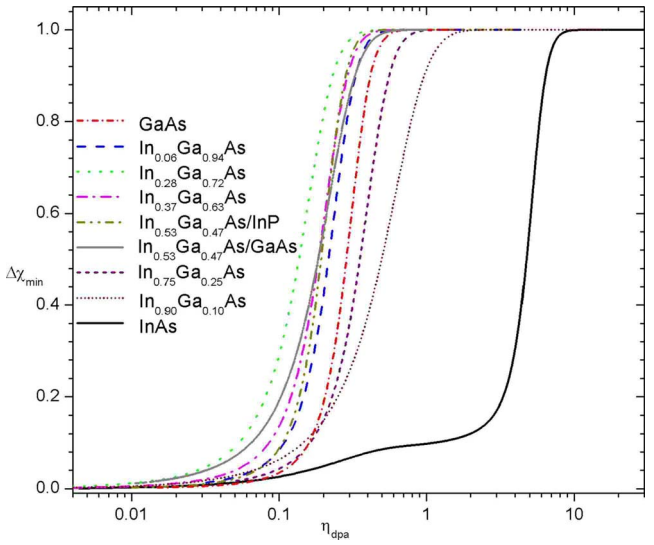

FIG. 3. (Color online) $\Delta\chi_{\min}$ as a function of the number of displacements per atom measured over the entire stoichiometry range x for $In_xGa_{1-x}As$. The plotted curves are fits to the experimental data points with the latter not shown for clarity.

lengths and Debye-Waller factors for a given pair of atoms set equal for the analysis of data at each K edge. For each bond type (Ga-As and In-As), the first nearest-neighbor (NN) and next-nearest-neighbor (NNN) distances were extracted from which the bond angles for each NNN configuration were then calculated. A complete multiple-scattering analysis was applied.

III. RESULTS AND DISCUSSION

With the exception of $In_{0.53}Ga_{0.47}As/InP$, all $In_xGa_{1-x}As$ layers were lattice mismatched with their respective substrates, generating misfit dislocations within the epitaxial layer during the growth process. For our given stoichiometries and substrates, a layer thickness of 0.1 μm exceeded the critical layer thickness reported by Andersson *et al.*[25] based on the pioneering work of Matthews and Blakeslee.[26] Dislocations observed using plan-view transmission electron microscopy (not shown) were of the 60° type oriented along the ⟨110⟩ direction consistent with the work of Edirisinghe *et al.*[27] To assess the potential influence of misfit dislocations on the amorphization kinetics, $In_{0.53}Ga_{0.47}As$ was grown on both lattice-matched InP and lattice-mismatched GaAs yielding epitaxial layers without and with dislocations, respectively. Ion implantation was then performed on both samples simultaneously followed by RBS-C measurements. Figure 2 shows $\Delta\chi_{\min}$ data as functions of η_{dpa} and the respective fits to the Hecking model. We note that such a comparison represents a "worst-case scenario" with the greatest lattice mismatch between ternary alloy and substrate for all samples examined in this study (as manifested by $Y_{\mathrm{unimplanted}}$ values of ~0.80 and ~0.05 for lattice-mismatched and matched samples, respectively). Nonetheless, equal values of critical η_{dpa} (0.18 ± 0.05 and 0.19 ± 0.04 η_{dpa} for $In_{0.53}Ga_{0.47}As$ with and without dislocations, respectively) were determined. The probability for direct-impact amorphization differed by a factor of 5 for samples with (1.03 ± 0.25) and without (0.23 ± 0.05) dislocations, while that for stimulated amorphization in the dislocated alloy (13.9 ± 2.4) was half that of the dislocation-free sample (24.12 ± 1.7). Clearly implantation-induced disorder production in $In_{0.53}Ga_{0.47}As$ is dominated by the stimulated amorphization regardless of the presence of misfit dislocations. Furthermore, both samples have lesser critical η_{dpa} values than InAs and GaAs (shown below) demonstrating that the rapid amorphization behavior did not result from the presence of pre-existing extended defects.

Figure 3 shows the fits for $\Delta\chi_{\min}$ as functions of η_{dpa} over the entire stoichiometry range and includes the two fits for $In_{0.53}Ga_{0.47}As$ presented in Fig. 2. For clarity, individual experimental points have not been included. It is readily apparent that the ternary alloys of $In_xGa_{1-x}As$ with stoichiometry $x \leq 0.53$ are amorphized at η_{dpa} values less than those required for both InAs and GaAs. In contrast, the In-rich alloys with $x \geq 0.75$ are rendered amorphous at η_{dpa} values intermediate between those necessary for the two binary extremes.

Values of critical η_{dpa} and the parameters P_a and A_s—the latter derived from fits to the $\Delta\chi_{\min}$ data—are plotted as functions of stoichiometry in Fig. 4. The quadratic fit to the η_{dpa} data indicates that an $In_xGa_{1-x}As$ alloy with stoichiometry of $x = 0.34 \pm 0.17$ is most easily amorphized. P_a is effectively independent of stoichiometry while A_s exhibits parabolic behavior with a maximum at $x = 0.28 \pm 0.18$. We note that the maximum in A_s is well correlated with the minimum in critical η_{dpa}. Clearly a stimulated amorphization process (A_s) is dominant relative to direct-impact amorphization (P_a) over the entire stoichiometry range and the differences in critical η_{dpa} value as a function of stoichiometry are governed by differences in the probability for stimulated amorphization.

To identify the atomistic configuration responsible for the amorphization behavior described above, we utilized EXAFS to probe the short-range order about each constituent atom

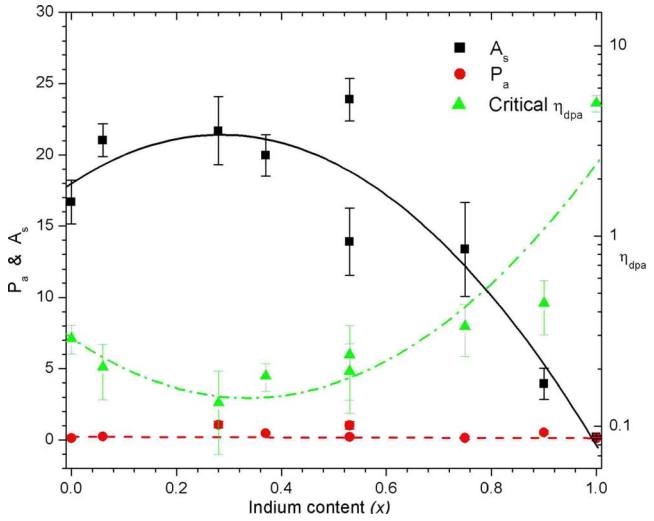

FIG. 4. (Color online) Critical n_{dpa} and probabilities for direct-impact (P_a) and stimulated (A_s) amorphizations as functions of stoichiometry for $In_xGa_{1-x}As$.

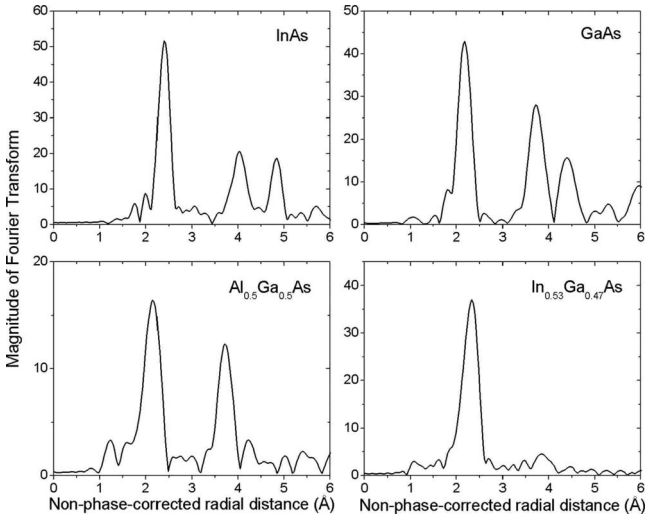

FIG. 5. Fourier-transformed As K-edge EXAFS spectra for unimplanted InAs, GaAs, $Al_{0.50}Ga_{0.50}As$, and $In_{0.53}Ga_{0.47}As$.

in the $In_xGa_{1-x}As$ samples. Two separate stoichiometry-dependent bond lengths were measurable, as consistent with the pioneering work of Mikkelsen and Boyce.[28] Following Cai and Thorpe,[29,30] we calculated topological rigidity parameters of 0.84 ± 0.01 and 0.73 ± 0.01 for the In-As and Ga-As bond-length distributions, respectively, in complete agreement with an average value of 0.80 reported previously.[16,17] These results indicate that the bimodal bond-length distribution of the $In_xGa_{1-x}As$ alloys is accommodated by both bond stretching and bond bending, though primarily via the latter as consistent with a higher force constant for bond stretching.

Figure 5 shows Fourier-transformed EXAFS spectra of unimplanted InAs, GaAs, $Al_{0.50}Ga_{0.50}As$, and $In_{0.53}Ga_{0.47}As$ measured at the common As K edge with the corresponding structural parameters listed in Table I. (The Fourier transforms shown in Fig. 5 are non-phase-corrected and hence the apparent radial distances do not correspond to the actual bond lengths. Corrected values of the latter are listed in Table I.) In general, a NN peak is apparent in all spectra at a non-phase-corrected radial distance of 2.1–2.3 Å. This shell is comprised of either In (in InAs), Ga (in GaAs), Al, and Ga (in $Al_{0.50}Ga_{0.50}As$) or In and Ga (in $In_{0.53}Ga_{0.47}As$) atoms (four in total). The amplitude of the NN peak is governed by multiple influences including an atomic-number dependence of the scattering factor for the atoms of the NN shell, a $(1/R^2)$ dependence to account for the loss of intensity of outgoing and scattered photoelectron waves (where R is the radial distance separating absorbing and scattering atoms), and the presence of structural disorder (characterized by the Debye-Waller factor). We measured only a slight increase in the Debye-Waller factors of the NN shell for $In_{0.53}Ga_{0.47}As$ relative to the binaries shown in Fig. 5 consistent with similar structural disorder in the bond-length distributions of the three materials.

Referring again to Fig. 5, we now consider the NNN peak at a non-phase-corrected radial distance of 3.7–4.0 Å which is comprised solely of As atoms (12 in total). Clearly the NNN peak for $In_{0.53}Ga_{0.47}As$ has a much smaller amplitude than InAs, GaAs, and $Al_{0.50}Ga_{0.50}As$ consistent with enhanced structural disorder in the bond-angle distribution. Comparing the two ternary alloys $Al_{0.50}Ga_{0.50}As$ and $In_{0.53}Ga_{0.47}As$, the greater NNN amplitude of the former is the result of the near equal Al-As and Ga-As bond lengths in $Al_{0.50}Ga_{0.50}As$ relative to the distinctly bimodal distribution

TABLE I. Bond lengths and bond angles for unimplanted InAs, GaAs, $Al_{0.50}Ga_{0.50}As$, $In_{0.53}Ga_{0.47}As$, and $In_{0.64}Ga_{0.36}P$ determined from EXAFS.

Material	Bond	Bond length (Å)	Angle	θ (deg)
InAs	In-As	2.609 ± 0.002	In-As-In	109.5 ± 0.2
GaAs	Ga-As	2.437 ± 0.002	Ga-As-Ga	109.7 ± 0.2
$Al_{0.50}Ga_{0.50}As$	Al-As	2.439 ± 0.022		
	Ga-As	2.444 ± 0.001	Ga-As-Ga	109.4 ± 0.4
$In_{0.53}Ga_{0.47}As$	In-As	2.591 ± 0.003	In-As-In	107.5 ± 0.3
	Ga-As	2.466 ± 0.003	Ga-As-Ga	113.4 ± 0.5
$In_{0.64}Ga_{0.36}P$	In-P	2.512 ± 0.003	In-P-In	108.7 ± 0.3
	Ga-P	2.361 ± 0.004	Ga-P-Ga	115 ± 0.7

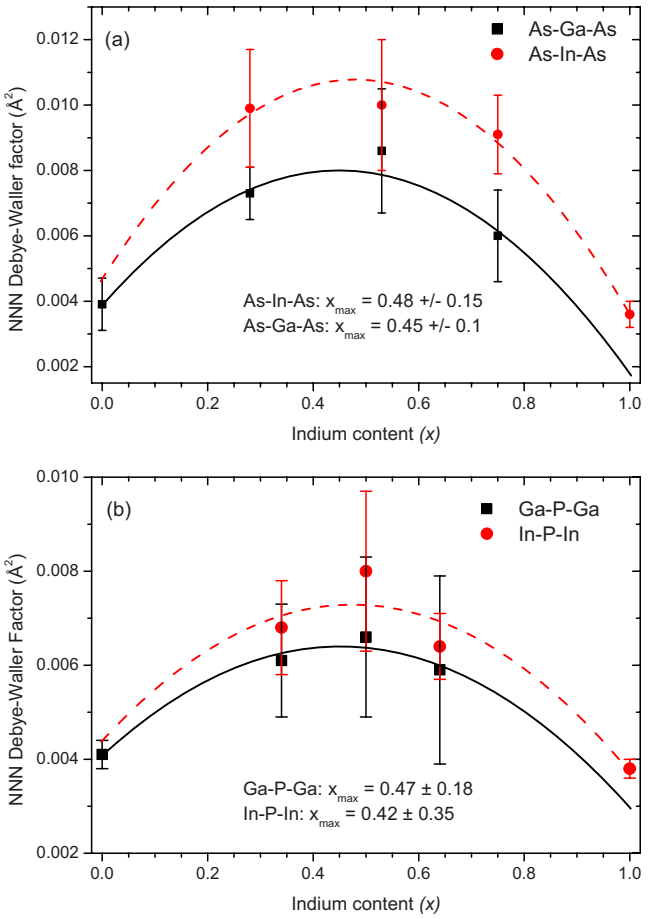

FIG. 6. (Color online) Debye-Waller factors for the next-nearest neighbor about (a) an As atom in unimplanted $In_xGa_{1-x}As$ and (b) about both In and Ga atoms in unimplanted $In_xGa_{1-x}P$, as functions of stoichiometry.

in $In_{0.53}Ga_{0.47}As$ as apparent from Table I. Accommodating two distinctly separate bond lengths on the zinc-blende lattice yields greater structural disorder in the interatomic distance distribution of the atoms comprising the NNN shell. We note that the strain-induced splitting of the NNN shell interatomic distances reported by Tormen *et al.*[31] is *not* present in our case given that the epitaxial layers were grown beyond the critical layer thickness and were then separated from the substrate prior to the EXAFS measurements. Included in Table I are the mean bond angles for the binary and ternary alloys shown in Fig. 5. The tetrahedral value was measurable for the two binaries, as expected, and for $Al_{0.50}Ga_{0.50}As$ where the bond-length distribution is effectively unimodal. In contrast, deviations from 109.5° are apparent for $In_{0.53}Ga_{0.47}As$. Note that the bond angles comprised of two long (short) In-As (Ga-As) bonds are less (greater) than the tetrahedral value, as one might intuitively expect.

Figure 6(a) shows Debye-Waller factors as functions of stoichiometry for the NNN shell about an As atom in $In_xGa_{1-x}As$. Structural disorder at the NNN shell in the ternary alloy is significantly greater than that of the two binaries with a maximum at $x=\sim 0.46$. Comparable results were reported by Jeong *et al.*[32] using complementary synchrotron-based x-ray diffraction to determine atomic-pair distribution functions. Examining the $In_xGa_{1-x}As$ alloys as functions of stoichiometry, they observed a broadening of the peak widths for the NNN shell due to an increased structural disorder with the latter a maximum for $x=\sim 0.5$. Our results agree well with those of Jeong *et al.*[32] These authors further demonstrated that atomic displacements on the In/Ga sublattice were isotropic and of lesser magnitude (~60%) than the highly directional (⟨100⟩ and ⟨111⟩) displacements on the As sublattice.

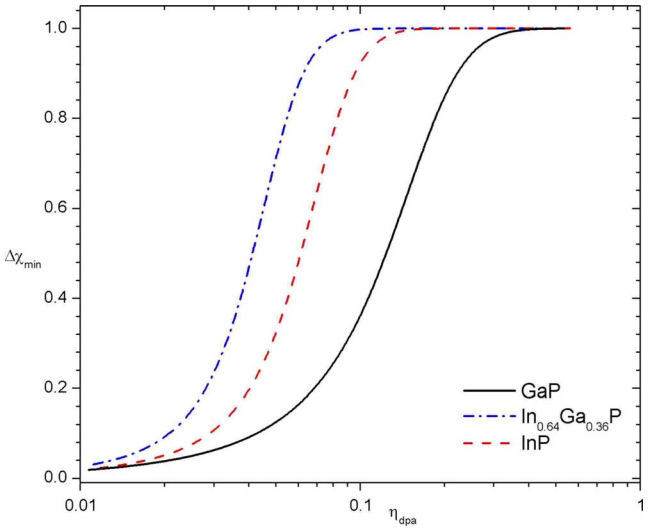

FIG. 7. (Color online) $\Delta\chi_{min}$ as a function of the number of displacements per atom comparing $In_{0.64}Ga_{0.36}P$, InP, and GaP.

Our study of the amorphization of the $In_xGa_{1-x}As$ alloys as functions of stoichiometry clearly demonstrates that the minimum in critical η_{dpa} is very well correlated with both the maxima in the probability for stimulated amorphization *and* the structural disorder at the next-nearest-neighbor shell. We thus suggest that structural disorder in the ternary alloys concentrated primarily in the bond-angle distributions serves as preferential sites for stimulated amorphization, rendering the $In_xGa_{1-x}As$ alloys amorphous at lesser critical η_{dpa} values than for both InAs and GaAs. The validity of this model can be tested with other ternary alloys exhibiting a bimodal bond-length distribution. For example, we have very recently reported an EXAFS study of the atomic-scale structure of $In_xGa_{1-x}P$ (Ref. 33) wherein two separate stoichiometry-dependent In-P and Ga-P bond lengths were measurable. Table I includes bond-length and bond-angle values for $In_{0.64}Ga_{0.36}P$, while Fig. 6(b) shows the NNN Debye-Waller factor for the $In_xGa_{1-x}P$ alloys as a function of stoichiometry. Clearly, $In_xGa_{1-x}P$ is structurally very similar to $In_xGa_{1-x}As$.

Figure 7 compares fits of $\Delta\chi_{min}$ as functions of η_{dpa} for $In_{0.64}Ga_{0.36}P$, InP, and GaP. Indeed $In_{0.64}Ga_{0.36}P$ is rendered amorphous at lower η_{dpa} values than required for either InP or GaP. A Hecking model analysis (not included) shows that the amorphization process is again dominated by the stimulated amorphization. Such results confirm the general applicability of our model.

IV. CONCLUSIONS

The kinetics for the ion-implantation-induced amorphization of $In_xGa_{1-x}As$ have been determined with RBS-C

over the entire stoichiometry range. Stoichiometries of $x = \sim 0.06-0.53$ were rendered amorphous at fluences lower than those required for either of the two binary extremes. The crystalline-to-amorphous phase transformation was dominated by a stimulated amorphization process; the probability for which was a maximum at the stoichiometry most easily amorphized. EXAFS measurements demonstrated the bimodal bond-length distribution characteristic of the $In_xGa_{1-x}As$ alloy was primarily accommodated on the zinc-blende lattice via bond bending with deviations from the tetrahedral bond angle readily apparent in the ternary alloy. Correlating EXAFS and RBS-C measurements, structural disorder and the probability of stimulated amorphization were both greatest at a common intermediate stoichiometry, where the ternary alloy was most easily amorphized. We thus suggest that the rapid amorphization kinetics of the $In_xGa_{1-x}As$ alloys results from structural disorder serving as preferential sites for stimulated amorphization. Accordingly, the structurally similar $In_xGa_{1-x}P$ alloys should—and did—exhibit comparable behavior.

ACKNOWLEDGMENTS

We thank H. H. Tan for the MOCVD growths and J. FitzGerald for the assistance with the electron microscopy. The Australian Research Council and Australian Synchrotron Research Program are gratefully acknowledged for financial support.

*Corresponding author. FAX: +61 2 6125 0511; zohair.hussain@anu.edu.au

[1] Andre Scavennec, M. Billard, P. Blanconnier, E. Caquot, P. Carer, Louis Giraudet, L. Nguyen, F. Lugiez, and Jean-Pierre Praseuth, Proc. SPIE **1362**, 331 (1991).
[2] J. John, L. Zimmermann, P. Merken, G. Borghs, C. A. Van Hoof, and S. Nemeth, Proc. SPIE **4820**, 453 (2003).
[3] J. John, L. Zimmermann, P. Merken, S. de Groote, G. Borghs, C. Van Hoof, S. Nemeth, and T. Colin, Proc. SPIE **5152**, 263 (2003).
[4] J. John, L. Zimmermann, S. Nemeth, T. Colin, P. Merken, S. Borghs, and C. A. Van Hoof, Proc. SPIE **4369**, 692 (2001).
[5] J. C. Boisvert, A. Masalykin, G. S. Kinsey, T. Isshiki, M. Haddad, R. Sudharsanan, X. Zheng, and J. C. Campbell, Proc. SPIE **5406**, 13 (2004).
[6] L. Zimmermann, J. John, M. de Weerd, M. Slaman, S. Nemeth, P. Merken, S. Borghs, and C. A. Van Hoof, Proc. SPIE **4288**, 77 (2001).
[7] S. Adachi, J. Appl. Phys. **58**, R1 (1985).
[8] *Properties of Lattice-matched and Strained Indium Gallium Arsenide*, EMIS Data Review Series No. 8 , edited by P. Bhattacharya (INSPEC, London, 1993).
[9] W. Wesch and M. C. Ridgway, Mater. Sci. Semicond. Process. **7**, 35 (2004).
[10] W. Wesch, E. Wendler, Z. S. Hussain, S. M. Kluth, and M. C. Ridgway, Nucl. Instrum. Methods Phys. Res. B **242**, 480 (2006).
[11] U. G. Akano, I. V. Mitchell, F. R. Shepherd, and C. J. Miner, Nucl. Instrum. Methods Phys. Res. B **106**, 308 (1995).
[12] K. M. Yu, in *Microstructural Processes in Irradiated Materials*, edited by S. J. Zinkle, G. E. Lucas, R. C. Ewing, and J. S. Williams, MRS Symposium Proceedings Vol. 540 (Materials Research Society, Pittsburgh, 1999), p. 79.
[13] K. M. Yu and L. Hsu, Appl. Phys. Lett. **69**, 824 (1996).
[14] J. F. Ziegler, Nucl. Instrum. Methods Phys. Res. B **219–220**, 1027 (2004).
[15] K. Gartner, K. Hehl, and G. Schlotzhauer, Nucl. Instrum. Methods Phys. Res. B **4**, 55 (1984).
[16] N. Hecking, K. F. Heidemann, and E. T. Kaat, Nucl. Instrum. Methods Phys. Res. B **15**, 760 (1986).
[17] W. J. Weber, Nucl. Instrum. Methods Phys. Res. B **166-167**, 98 (2000).
[18] S. Arscott, P. Mounaix, and D. Lippens, J. Vac. Sci. Technol. B **18**, 150 (2000).
[19] A. R. Clawson, Mater. Sci. Eng. R. **31**, 1 (2001).
[20] G. C. DeSalvo, W. F. Tseng, and J. Comas, J. Electrochem. Soc. **139**, 831 (1992).
[21] C. Greus, A. Forchel, J. Straka, K. Pieger, and M. Emmerling, J. Vac. Sci. Technol. B **9**, 2882 (1991).
[22] Y. Sasaki, T. Katayama, T. Koishi, K. Shibahara, S. Yokoyama, S. Miyazaki, and H. Hirose, J. Electrochem. Soc. **146**, 710 (1999).
[23] M. Newville, J. Synchrotron Radiat. **8**, 322 (2001).
[24] B. Ravel and M. Newville, J. Synchrotron Radiat. **12**, 537 (2005).
[25] T. G. Andersson, Z. G. Chen, V. D. Kulakovskii, A. Uddin, and J. T. Vallin, Appl. Phys. Lett. **51**, 752 (1987).
[26] J. W. Matthews and A. E. Blakeslee, J. Cryst. Growth **27**, 118 (1974).
[27] S. P. Edirisinghe, A. Staton-Bevan, P. N. Fawcett, and B. A. Joyce, J. Vac. Sci. Technol. B **13**, 967 (1995).
[28] J. C. Mikkelsen and J. B. Boyce, Phys. Rev. B **28**, 7130 (1983).
[29] Y. Cai and M. F. Thorpe, Phys. Rev. B **46**, 15879 (1992).
[30] Y. Cai and M. F. Thorpe, Phys. Rev. B **46**, 15872 (1992).
[31] M. Tormen, D. De Salvador, A. V. Drigo, F. Romanato, F. Boscherini, and S. Mobilio, Phys. Rev. B **63**, 115326 (2001).
[32] I. K. Jeong, F. Mohiuddin-Jacobs, V. Petkov, S. J. L. Billinge, and S. Kycia, Phys. Rev. B **63**, 205202 (2001).
[33] C. S. Schnohr, L. L. Araujo, P. Kluth, D. J. Sprouster, G. J. Foran, and M. C. Ridgway, Phys. Rev. B **78**, 115201 (2008).